The effect of extensional flow on the evaporative assembly of a donor-acceptor semiconducting polymer

*Shayla Nikzad[1], Hung-Chin Wu[1], Ging-Ji Nathan Wang[2], Hongping Yan[1], Sebastian A. Schneider[2,3], Michael F. Toney[3], Zhenan Bao[1,]**

[1] Department of Chemical Engineering, Stanford University, Stanford, California 94305, United States

[2] Department of Chemistry, Stanford University, Stanford, California 94305, United States

[3] Stanford Synchrotron Radiation Lightsource, SLAC National Accelerator Laboratory, Menlo Park, California 94025, United States

* Correspondence to: zbao@stanford.edu

KEYWORDS: conjugated polymer, polymer alignment, solution processing, extensional flow, field-effect transistor

ABSTRACT

The ability to deposit polymer semiconductors (PSCs) over a large area at near ambient conditions makes them exciting candidates for low-cost large area electronic applications. Given the sensitivity of the charge carrier mobility in PSCs to the nature of their deposition from solution, a mechanistic understanding of deposition processes is essential for enhancing and controlling a PSC's electrical performance. Polymer chain alignment has been largely posited as a strategy for improving electrical performance of PSCs. In this work the ability of a micropillar shearing blade to align polymer chains of poly(2,5-bis(2-octyldodecyl)-3,6-di(thiophen-2-yl)diketopyrrolo[3,4-c]pyrrole1,4-dione-alt-thieno[3,2-b]thiophen) (DPP-TT) during solution shearing by increasing extensional flow is investigated. A sufficiently strong extensional flow field is found to be capable of aligning polymer chains and inducing crystallization. Such an alignment of crystallite domains is observed to be correlated to increased charge carrier mobility, but the effect of such an alignment on charge transport is dependent on deposition conditions. Furthermore, the ability of polymer chains to be aligned by using extensional flow, and the effect of such an alignment on subsequent charge transport, is highly dependent on polymer chain length due to changes in both solution state properties and charge transport mechanisms.

1. INTRODUCTION

Polymer organic semiconductors (PSCs) are lightweight, mechanically compliant, easily tunable through chemical synthesis, and capable of being deposited over large area, making them excellent candidates for inexpensive printable electronics with functionalities currently underserved by conventional inorganic semiconductors. Unlike their inorganic counterparts, in solid films, PSCs are held together by weak Van der Waals and π-π interactions, resulting in a heterogeneous microstructure, which can be easily modulated during deposition. Because of the relationship between the microstructure and PSC charge transport there exists a strong correlation between electrical properties and deposition method.[1–3]

Solution shearing is a commonly studied method for depositing PSCs due to its amenability to high throughput roll-to-roll processing.[4–7] A variety of methods have been used in conjunction with solution shearing to manipulate the thin film microstructure of PSCs. These methods include molecular confinement using a nanostructured surface,[8,9] use of an applied field,[10] and flow-controlled methods, which are the topic of this manuscript.

During solution shearing, polymer chains are subject to a boundary-driven flow generated by the coating blade. One way to control the flow profile during solution shearing is by introducing lithographically patterned structures onto the coating blade. Micropillar shearing blades have been studied for the deposition of small molecule organic semiconductors.[11–14] PSC assembly into the thin film state is affected by polymer chain conformation and dynamics, making the morphological control of PSCs during deposition mechanistically distinct from that of small molecule organic semiconductors. In PSC deposition, the use of micropillar blades has been studied much less

frequently. Namely, it has been shown that deposition using a micropillar blade can result in increased thin film crystallinity.[15,16]

The discovery of new materials that exhibit relatively low crystallinity while still achieving excellent charge transport indicate the importance of an elongated and planarized polymer backbone in a fast charge transport.[17] Both theoretical and experimental work suggest that an "ideal" semiconducting thin film morphology requires efficient intrachain charge transport via long rigid polymer chains, connecting neighboring crystallites.[18–23] This model suggests that aligning and extending polymer chains may be an effective strategy for increasing the efficiency of charge transport by reducing the number of slow charge carrier "hops" required for percolation through the film.

Most recently, our group used a micropillar blade to align stretchable polymer/elastomer blended nanostructures in order to facilitate faster charge transport along the aligned polymer nanostructures.[24] However, the film formation mechanism in this case was dependent on the phase separation of polymer chains from the surrounding elastomer into nano-scale fibers. Thus, it is worthwhile to investigate if a micropillar blade can be used to produce a nano-scale polymer chain alignment in neat polymer films (i.e. with only single semiconducting polymer), given the uniqueness of the film formation mechanism compared to a binary system (i.e. semiconducting polymer with elastomer).

Subsequently, in this work the ability of shear and elongation flow fields created by the micropillar blade, as shown in **Figure 1a**, to extend and align polymer chains and facilitate efficient charge transport pathways is assessed using a diketopyrrolopyrrole-based polymer, poly(2,5-bis(2-octyldodecyl)-3,6-di(thiophen-2-yl)diketopyrrolo[3,4-c]pyrrole-1,4-dione-alt-

thieno[3,2-b]thiophen) (DPP-TT). At sufficiently high shearing speeds, the use of a micropillar blade is indeed effective in increasing polymer chain alignment and thin film crystallinity. Such an alignment is, in addition, dependent on polymer molecular weight/chain length. Additionally, a non-direct correlation between bulk polymer chain alignment and charge transport anisotropy is observed, suggesting that polymer chain alignment does not always promote faster charge transport, which may be the result of potential disruption of order from the top film interface.

2. RESULTS

2.1 Polymer Chain Alignment

Strong flow fields (both shear and extensional) have been shown to induce polymer crystallization through the elongation and alignment of polymer chains.[25–30] During solution shearing, polymer alignment can be induced using shear flow created by the coating blade.[31–33] More recently, our group has discovered that by altering the flow-profile during coating using micron-scale structures, alignment can be further increased for semiconductor-elastomer nanostructures.[24] In this work, we assess the ability of extensional flow created using a micropillar blade to induce alignment in neat polymer films. Specifically, rectangular pillars spaced 6 μm apart are patterned onto the shearing blade (**Figure 1a**). As depicted in **Figure 1a**, during coating an extensional flow field will be induced by forcing polymer solution from a large cavity (millimeter-scale) to a much smaller cavity (micron-scale). Such an extensional flow is expected to result in the elongation of polymer chains present in solution.

To test the ability of extensional flow generated in this manner to produce polymer chain alignment, films of DPP-TT were deposited from a chlorobenzene solution onto an n-octadecyltrimethoxysilane (OTS) treated Si/SiO_2 substrate using the micropillar blade. Reference

films were deposited using a silicon coating blade with no micropillars. Shearing speeds between 0.2 and 8 mm/s were tested.

Two characteristic coating regimes are typically observed in solution shearing. The evaporative regime occurs at lower shearing speeds and is characterized by slow solvent evaporation and decreasing film thickness with increasing shearing speeds. The classically-termed Landau Levich (LL) regime occurs at higher coating speeds and is characterized by faster solvent evaporation rates and increased film thickness with increasing speed.[34] The coating regime in which a film is deposited may greatly affect the final thin film morphology and polymer chain alignment due to changes in evaporation rate and overall time of drying. In this study, films deposited in both the evaporative and LL regime were characterized. Based on measured film thickness, the transition from the evaporative regime to the LL regime begins to occur after the blade speed increases to above ~1 mm/s (**Figure 1b**). It should be noted that the film thicknesses obtained using the micropillar and reference blades were comparable across different shearing speeds, eliminating any additional effects that may result from variable film thickness.

Bifringence observed from polarized optical microscopy (POM) images indicates macroscopic alignment of the solution sheared films deposited using both the reference and micropillar blades (**Figure 1c**). Additionally, because the absorption transition dipole moment lies predominantly along the polymer backbone, macroscopic polymer chain alignment can be determined by comparing the UV-Visible absorption spectra of light polarized both parallel (i.e. $\varphi = 0^{o}$) and perpendicular (i.e. $\varphi = 90^{o}$) to the direction of coating.[35,36] The polymer backbone absorption peak (600-900 nm) exhibits two vibronic bands, with the lower energy peak (0-0) typically attributed to polymer aggregation.[37] Here, the dichroic ratio (DR) is taken to be the 0-0 peak intensity in the

direction along (φ =0°) the shearing direction over the direction perpendicular to the shearing direction (φ=90°). Therefore, a DR greater than 1 indicates polymer chain alignment in the direction of coating (**Figure 1d**). Calculations of the DR based off the higher energy vibrionic band (0-1 peak) showed trends consistent with those for the 0-0 peak. An increase in overall polymer chain alignment was observed across the tested shearing speeds for films coated using both the reference and micropillar blades (**Figures 1d** and **e**). At shearing speeds above 1 mm/s, use of the micropillar blade appears to correspond to a modest increase in polymer chain alignment in comparison to the films coated using the reference blade (6-24% increase). The relatively small difference in optical absorption may be due to the relatively low crystalline fraction in DPP materials. Since the elongation flow field is expected to increase from 1mm/s to 8 mm/s, this result suggests that elongational flow may play a role in enhancing polymer chain alignment. Such an enhancement in alignment may occur through the alignment of polymer nanoaggregates or through shear-induced polymer chain elongation and subsequent crystallization of aligned polymer chains. The detailed mechanism requires further investigation with morphological characterization as detailed below. Furthermore, a shearing blade with a reduced pillar spacing of 3 μm was tested and yielded comparable polymer chain alignment to that of the blade with 6 μm spacing, despite an anticipated increase in shear and extensional flow (**Figure S2**). For smaller mircopillars a greater pressure difference is required to drive fluid through the micropillars, rather than below them. The lack of further alignment upon reducing pillar spacing may be a result of decreased driving force for fluid to travel through the micropillars, rather than underneath them. Moreover, the inability of more closely spaced micropillars to further align polymer chains has been observed previously[24].

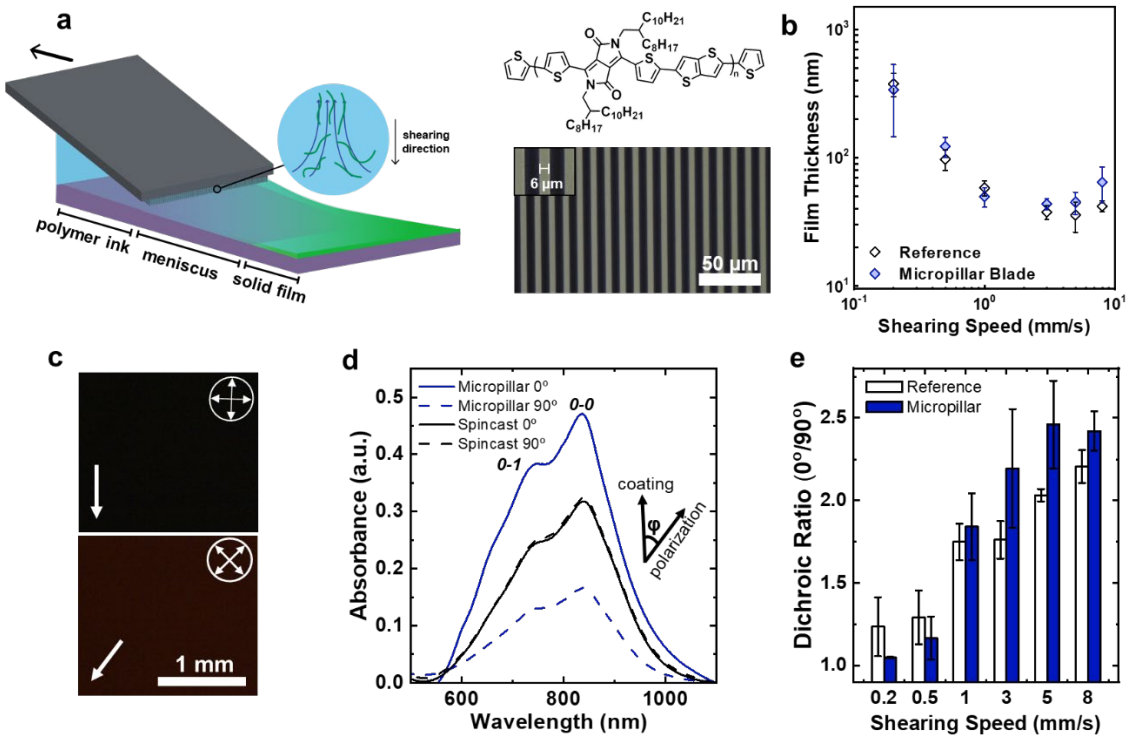

Figure 1. (a) Micropillar shearing apparatus. Inset shows polymer chains exposed to extensional flow via micropillars, resulting in polymer chain extension and alignment. The blue arrows represent the flow field created by the micropillar channel. The green lines represent polymer chains. Chemical structure of DPP-TT polymer. Optical microscope image of micropillar blade used. Both pillars and pillar spacing are 6 µm. (b) Film thickness for films deposited using micropillar and reference blades. (c) Polarized optical micrograph of thin film sheared at 3 mm/s. (d) Normalized absorption spectra for films sheared using a micropillar shearing blade at 8 mm/s versus a spincast film of DPP-TT, which is isotropic. (e) The tabulated dichroic ratio for reference

and micropillar blade films determined based on the intensity of the 0-0 vibronic peak parallel and perpendicular to shearing.

2.2 Morphological Characterization

In order to examine how the changes to the flow profile alter the crystallization kinetics, and thus the film morphology, during solution shearing, the surface and bulk crystalline textures were characterized using atomic force microscopy (AFM) and grazing-incidence x-ray diffraction (GIXD), respectively.

GIXD was employed to develop further understanding of polymer chain alignment in this system by probing crystallite orientation. We define the anisotropy of crystallinity as the ratio of the diffraction intensity of the π-π stacking (010) from diffraction patterns taken with the beam path parallel ($\varphi=0^{o}$) and orthogonal (i.e. $\varphi=90^{o}$) to the shearing direction (**Figures 2a** and **b**). Consistent with optical measurements of alignment, we see that crystallite alignment increases with increasing coating speed (**Figure 2c**). Films coated using the micropillar blade exhibited significant increases in polymer chain alignment, with films coated at 8 mm/s showing a nearly 3-fold increase in crystallite alignment of subsequent films, much larger than the optical DR.

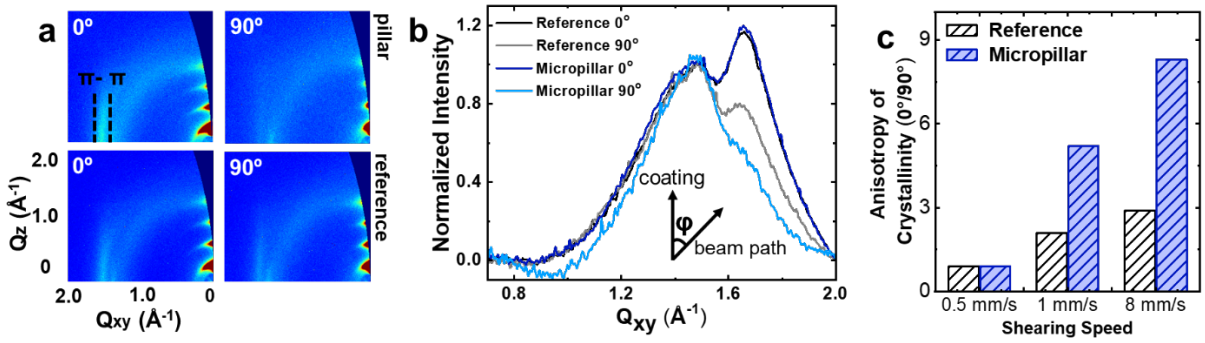

Figure 2. Summary of crystallite anisotropy. (a) Normalized diffraction patterns taken in the direction parallel (0°) and perpendicular (90°) to shearing for reference and micropillar films deposited at 8 mm/s (b) 1D profiles of diffraction intensity for the (010) peak taken parallel and perpendicular to shearing at 8 mm/s. (c) Calculated anisotropy of crystallinity based on the π-π stacking intensity (i.e. (010) diffraction peak intensity) parallel and perpendicular to coating.

It has been demonstrated that the presence of extensional and shear flow fields, both during rheological experiments and deposition, is capable of inducing crystallization in PSCs.[15,16,29,30] Such an increase in crystallization is believed to be the result of a reduced entropic barrier to crystallization caused by the alignment and elongation of polymer chains. Given the clear observations of polymer chain alignment, the correlation between polymer chain alignment and thin film crystallinity was investigated.

X-ray diffraction intensity can be used to compare the relative crystallinity of films of the same material.[38] In this case the relative degree of crystallinity (rdoc) of micropillar and reference blade-deposited thin films was assessed by comparing the intensity of the first-order lamella (100) diffraction peak.[16] Diffraction patterns from -90 to 90° with respect to the coating direction were taken (**Figure 3a**). The integrated intensity of the contributions from each angle φ represents the

rdoc of a given film. Indeed, at sufficiently high shearing speeds, an increase in rdoc is observed (**Figure 3b**). This observation is consistent with the hypothesis that polymer alignment is shear-induced, which should also induce crystallization. At a high coating speed (8 mm/s) the coating is entering the LL regime (**Figure 1b**), where stochastic crystallization starts from the liquid-air interface. The fact that both alignment and rdoc are higher for the micropillar coated film suggests shear-induced alignment and crystallization are at play.

It can be seen that the trend in rdoc for films deposited using the micropillar blade is qualitatively different than the trend observed for films deposited using the flat reference (**Figure 3b**). For reference films, rdoc decreases with increasing shearing speed. We attribute such a decrease in rdoc to changes in the drying dynamics that occur with increasing shearing speed. It has been observed previously that films deposited in the LL regime exhibit decreased crystallinity, potentially resulting from rapid crystallization at the wet film surface, which suppresses the overall crystallization of the underlying films.[38] Conversely, for films coated using the micropillar blade, an increase in crystallinity was observed with increasing shearing speed, suggesting that not only is a sufficiently strong extensional flow capable of inducing polymer crystallization, the use of an elongation flow field allows for crystallinity to be maintained into the LL regime. However, it should be noted that at 1 mm/s, the rdoc for films deposited using the micropillar blade is lower than reference blade. This difference may be due to the positioning of the reference blade in this study. Both the micropillar and reference blades were placed 15 μm from the substrate. This reference blade placement was chosen to ensure that observed phenomena was not the result of simply increasing shear flow in the areas below the pillars. However, such a placement of the reference blade may result in the presence of a larger out-of-plane shear stress than that of the micropillar blade given that 50% of the micropillar blade is 35 μm from the surface rather than 15

(from lubrication theory out-of-plane shear stress is proportional to the gap height for a flat shearing blade).[31] Thus, the observed increase in crystallinity shown for the reference blade at 1 mm/s may be due to a shear-induced crystallization mechanism, which may be dominant when the elongation flow field is not yet large enough to elongate polymer chains and induce crystallization.

Additionally, surface morphology was analyzed using Atomic Force Microscopy (AFM). A fibral morphology that begins to dissipate after a shearing speed of 3 mm/s was observed from AFM phase images, as depicted in **Figure 3c**. There is not a discernable difference in AFM images taken from micropillar films versus reference films (**Figure S4)**. Given that only the surface of the material is probed, the lack of difference may be a result of interfacial misorientation at the air-

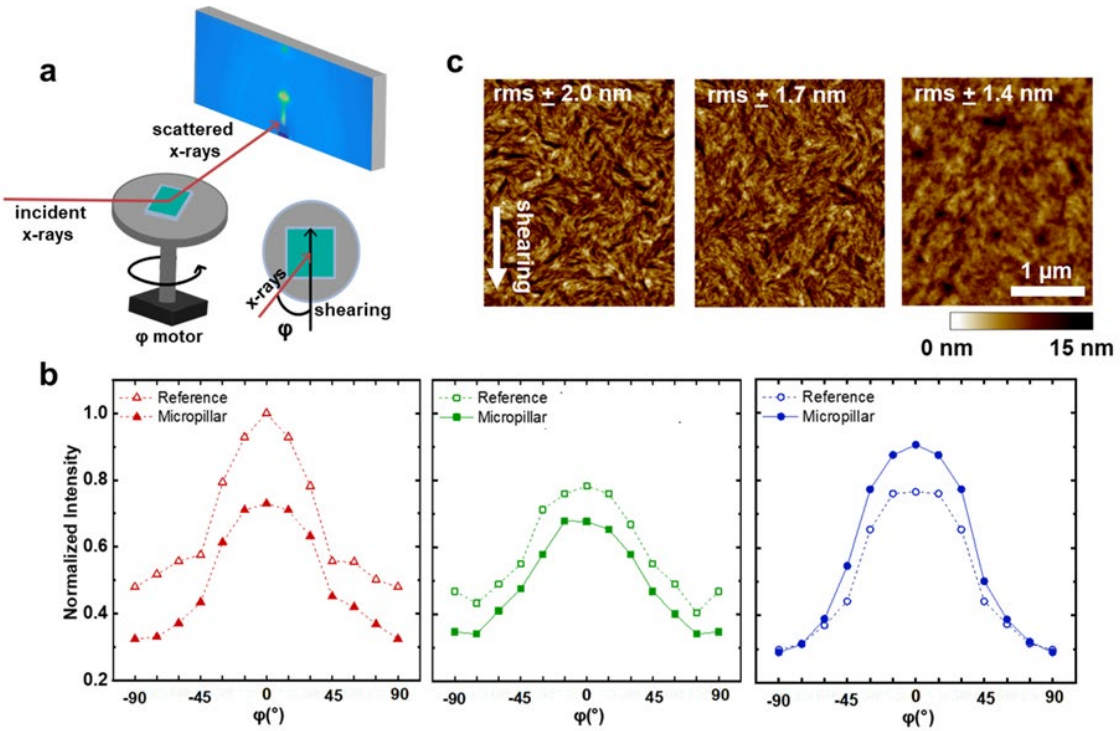

film interface due to rapid solvent evaporation. Indeed, highly anisotropic films of solution sheared DPP that do not display strong indicators of alignment at the top film interface have been reported.[31] Moreover, gradients of alignment have been observed in solution sheared DPP-based films previously.[40]

Figure 3. Characterizations of the thin film bulk and surface texture. (a) Schematic of rotational GIXD measurement to determine relative degree of crystallinity (rdoc) (b) Normalized (100) peak intensity versus sample rotation angle, φ for reference and micropillar films deposited at 1 mm/s, 3 mm/s, and 8 mm/s from left to right. (c) AFM phase images of films deposited using micropillar blade labeled with calculated roughness deposited at 0.5, 1, and 8 mm/s from left to right.

2.3 Charge Transport

Bottom gate/top contact transistors were fabricated using the structure shown in **Figure 4a**. Mobility was probed in the directions parallel and perpendicular to shearing. Mobility values in the direction parallel to coating ranged from 0.88 to 1.11 $cm^2/V/s$. The observed charge transport weakly anisotropic with all films deposited at a coating speed lower than 5 mm/s exhibiting reduced mobility in the direction perpendicular to shearing. Films deposited using both the reference and micropillar blade exhibited a local maximum in mobility, on current, and mobility anisotropy at a coating speed of 1 mm/s (**Figures 4b, c**, and **d**), despite a monotonic increase in polymer chain alignment observed across all shearing speeds from both optical and X-ray characterization. Insignificant differences in mobility between the reference and micropillar blade is observed (**Figure 4e**). The device characteristics for all films deposited using the micropillar blade are summarized in **Table 1**.

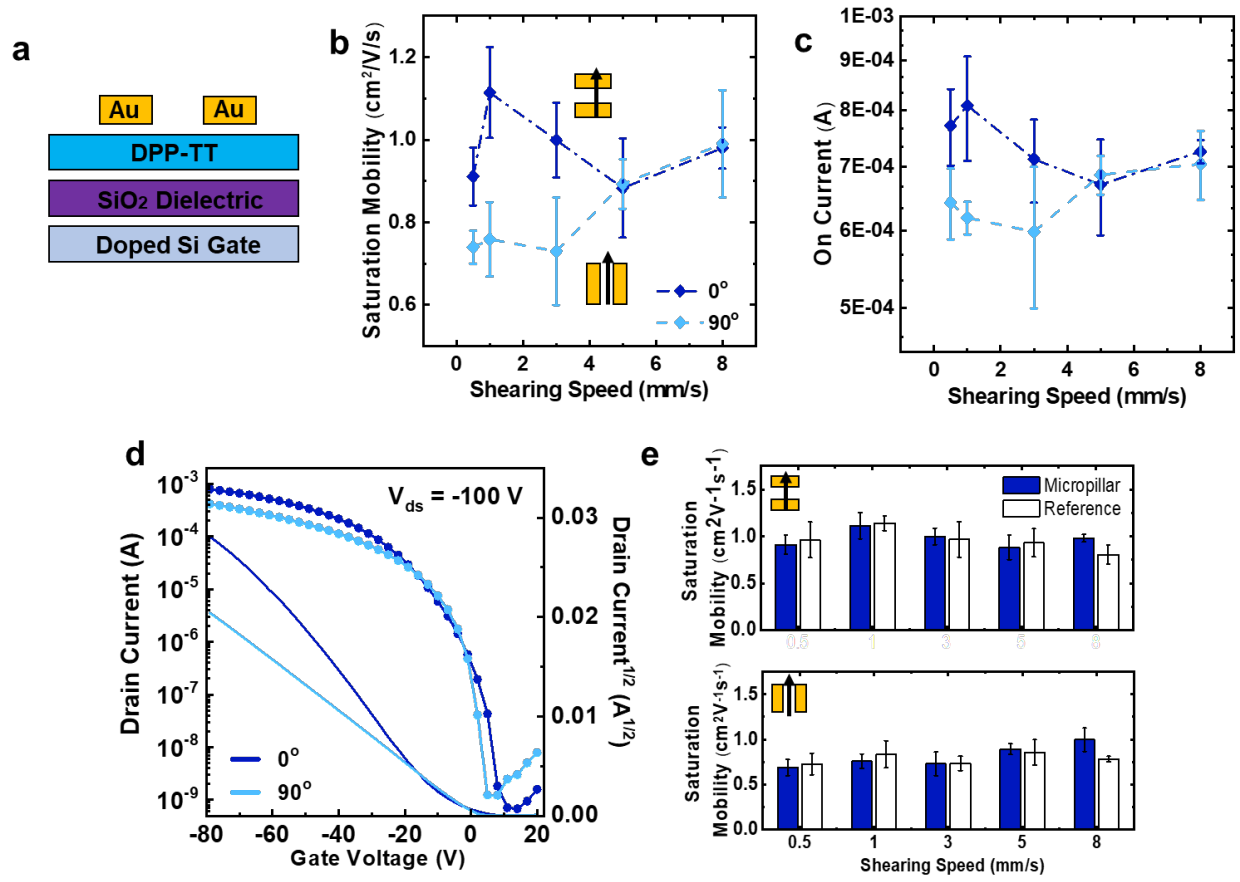

Figure 4. Summary of charge transport characteristics. (a) Schematic of device configuration. (b) Mobility and (c) on current parallel (dark blue) and perpendicular (light blue) to shearing for micropillar blade across tested shearing speeds. (d) Representative transfer curves parallel and perpendicular to shearing for micropillar film deposited at 1 mm/s. (e) Mobility comparison of micropillar and reference films across shearing speeds in directions parallel (top) and perpendicular (bottom) to shearing

Table 1. Device performance parameters for devices fabricated using micropillar blade

Shearing Speed (mm/s)	$\mu_h^{\parallel}$ ($cm^2/V/s$)	V_{th} (V)	I_{on}/I_{off}	$r_{ave}^{a)}$	$\mu_h^{\parallel}/\mu_h^{\perp}$
0.5	0.91 ± 0.07	-2 ± 2	10^5-10^6	0.89	1.3
1	1.11 ± 0.11	-5 ± 4	10^6-10^7	0.73	1.5
3	0.99 ± 0.09	-5 ± 2	10^6-10^7	0.75	1.4
5	0.88 ± 0.12	-4 ± 4	10^5-10^7	0.67	1.0
8	0.98 ± 0.05	-6 ± 3	10^6	0.74	1.0

a) average reliability factor[50]

Figure 5 summarizes the morphological evolution of films sheared using the micropillar and reference blades. From speeds of 0.5 to 1 mm/s, polymer chains transition from their initial isotropic orientation to an aligned state, which may potentially result in increased charge carrier mobility and increased mobility anisotropy between parallel and perpendicular directions. In this range, though polymer alignment appears to effect charge transport, the reference and micropillar blade coated films likely exhibit statistically insignificant differences in mobility due to the similar degree of alignment produced by both blades at these speeds (**Figure 1d**). At above 1 mm/s the reference films become slightly more aligned and less crystalline whereas films deposited using the micropillar blade become significantly more aligned and more crystalline in the direction of coating.

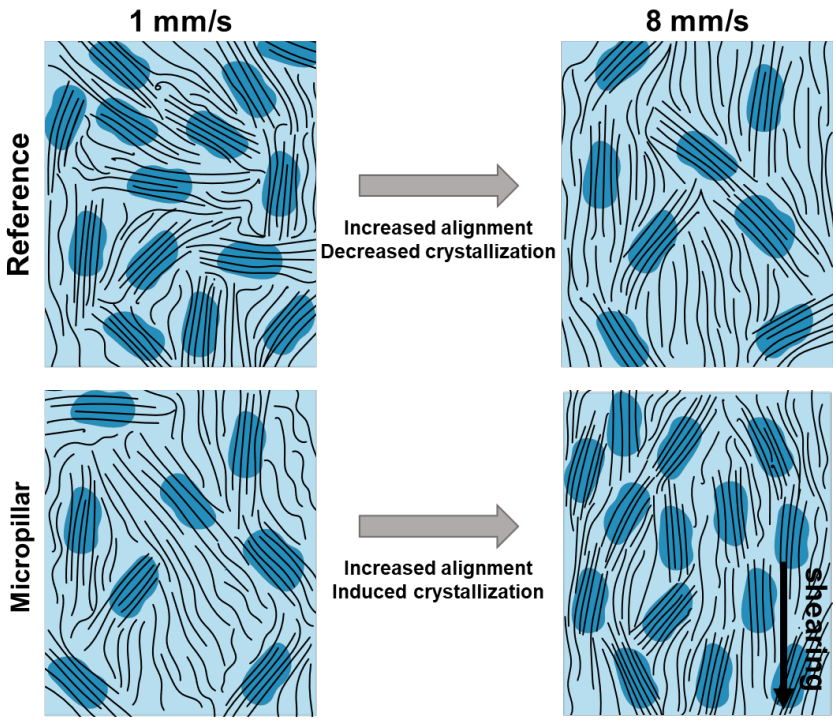

Figure 5. Summary of thin film morphology for reference (top) and micropillar (bottom blades). At low shearing speeds (1 mm/s) the micropillar blade produces greater polymer chain alignment despite being less crystalline than the reference blade. At 8 mm/s films deposited using the micropillar blade are both more crystalline and significantly more aligned than reference films.

Despite such increases in polymer chain alignment, a decreases of both mobility and mobility anisotropy are observed. These decreases may be due to changes in the drying kinetics during film formation. That is, after the transition to the LL regime, the rate of evaporation increases, which may result in stochastic nucleation at the interface, disrupting polymer chain alignment developed using flow[38]. Give that the films deposited in this study are relatively thin, such a disruption in alignment propagating from the top surface may inhibit anisotropic charge transport and overall charge carrier mobility. Indeed, from AFM height and phase images a change in the surface morphology characterized by a decrease in roughness was observed (**Figure 3b**).

It is worth highlighting that despite clear qualitative differences in thin film crystallinity of the micropillar and reference films, charge transport behavior remains qualitatively similar, suggesting that alignment may be a more effective strategy for facilitating charge transport than increasing crystallinity for the tested polymer system. This is not surprising as similar observations have been reported previously. It has been suggested that having good connectivity between small crystallites through tie chains is more important than having a large crystalline fraction in the film.[18,19] Our results are consistent with these conclusions.

2.4 Effect of Polymer Chain Length

Both theoretical and experimental work have shown that increasing polymer molecular weight correlates to an increase in charge carrier mobility, which then asymptotes or declines at a sufficiently high molecular weight.[41–44] It has been broadly hypothesized that low molecular weight polymers contain polymer chains that are too short to connect neighboring crystallites, preventing charge percolation along the polymer backbone. As molecular weight is increased, percolation along the polymer backbone becomes possible as "tie chains" between neighboring crystallites begin to form, resulting in observed increases in charge transport. However, as molecular weight becomes too high, mobility begins to saturate or decline due to kinks and entanglements in the polymer backbone, which have been suggested both theoretically and experimentally to serve as charge carrier traps.[45,46]

Given the implicated importance of polymer chain length on charge transport as well as the tendency for the solution state characteristics of PSCs to change with molecular weight (e.g. aggregation state and entanglement state),[47,48] DPP-TT of both lower molecular weight (Mn = 10 kDa) and higher molecular weight (Mn = 32 kDa) than the polymer studied in the above

experiments (Mn = 17 kDa) was deposited using the micropillar shearing blade. The solution viscosity for each tested molecular weight was tuned to ensure comparable film thickness and prevent any shifting in the transition point between the evaporative and LL regimes (**Figure S6a**).

From polarized UV-Vis. the median molecular weight polymer exhibits the greatest degree of polymer chain alignment while the high molecular weight polymer shows the lowest observed alignment of the molecular weights tested (**Figure 6a**). GIXD measurements reveal similar alignment behavior to the behavior observed optically (**Figure 6a**). The observed trends in alignment may be due to the ideal properties in the solution state of the 17 kDa polymer. Numerous works have pointed to the importance of solution state aggregates in creating an aligned microstructure during unidirectional coating.[31,48,49] In general, increasing molecular weight increases solution state aggregation.[46,47] Solution state UV-Vis absorption spectra was collected to confirm that aggregation in solution did indeed increase with molecular weight (**Figure S6b**). Thus, given its more aggregated state in solution, it is possible that the 17 kDa polymer is more easily aligned than the 10 kDa polymer. However, despite clearly increased aggregation in solution, the 32 kDa polymer shows the lowest level of alignment among the three tested molecular weights. Additionally, while the alignment of the 17 kDa and 10 kDa polymer appears to be monotonically increasing with increasing shearing speed, the alignment of the 32 kDa polymer asymptotes at shearing speeds higher than 1 mm/s. These observations in combination suggest that, for the high molecular weight polymer, there may be a frustration of polymer chain alignment after a certain speed, which could result from either the presence of chain entanglements or the existence of aggregates in solution that are too large, resulting in a disturbance of the assembly into the thin film state.

Again, charge carrier mobility in the direction parallel and perpendicular to coating was investigated for all molecular weights tested. Parallel and perpendicular mobility values collected from films deposited using the micropillar blade at 1 mm/s are shown in **Figure 6b**. For the low molecular weight polymer, charge transport is isotropic. The mobility of the 10 kDa polymer was consistent across shearing speeds and consistently isotropic (**Figure S9a**). Such an isotropic charge transport behavior is consistent with a morphology in which polymer chains are too short to create tie chains between neighboring crystallites, resulting in a charge transport that is highly isotropic despite some observed polymer chain alignment. Despite quantitatively lower alignment, the 32 kDa polymer showed higher mobility anisotropy than the median molecular weight polymer (**Figure 6c)**. Again, these observations are consistent with a charge transport model where tie chains between neighboring molecules are essential for efficient charge percolation. While the 32 kDa polymer may exhibit a lower degree of alignment, a higher fraction of tie molecules may amplify the effect of alignment. Similar to the 17 kDa polymer, the 32 kDa polymer exhibited charge transport anisotropy which increases up to 1 mm/s before becoming isotropic, again suggesting a competition between drying kinetics and flow-induced alignment. Unlike the median molecular weight polymer, the charge carrier mobility of the 32 kDa polymer decreases with increasing shearing speed for all shearing speeds greater than 0.5 mm/s (**Figure S9b**). This further implies the presence of large aggregates or chain entanglements that inhibit alignment of the high molecular weight polymer. A competition between flow induced alignment and polymer chains that are too strongly coupled to one another (either through aggregation or entanglement) may result in an overall disordering of the thin film state, lowering mobility. Thus it is possible that, while charge transport remains anisotropic, the overall charge carrier mobility of such a film is reduced.

While increasing polymer molecular weight has been broadly posited as strategy to improve PSC performance, very few works have studied PSC molecular weight in the context of unidirectional coating. Here we show that an intermediate molecular weight polymer is not only the most conducive to alignment under flow, but also possess the highest charge carrier mobility when deposited using solution shearing. Indeed, in studies of the meniscus guided coating of other donor-acceptor conjugated polymers,[51] as well as P3HT,[32] others have observed a local maximum in electronic performance at intermediate molecular weight. The aggregate of these findings suggest that while increasing molecular weight may be an effective means for increasing connections between crystalline regions with faster charge transport in spincast films, further understanding of the solution state properties of high molecular weight PSCs is necessary to translate this advantage to films deposited using more industrially relevant, unidirectional coating methods.

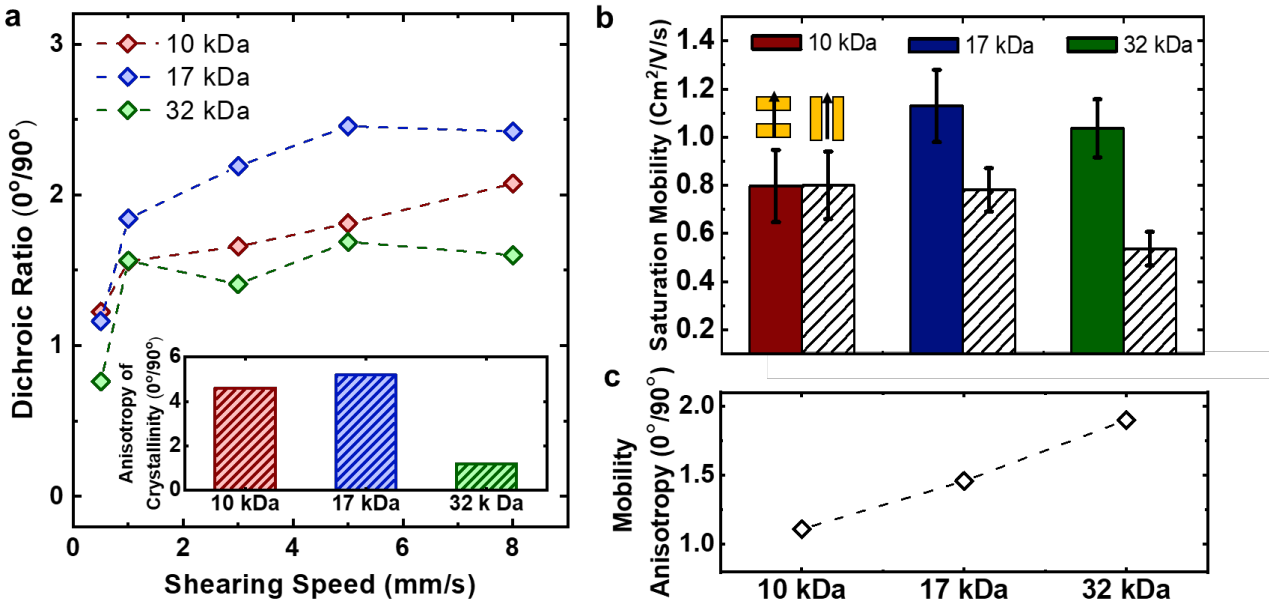

Figure 6. Effect of molecular weight. (a) Dichroic ratio for films deposited using the micropillar shearing blade. Inset shows crystallite anisotropy for films coated at 1 mm/s. (b) Mobility parallel

and perpendicular to shearing at a shearing speed of 1mm/s. Colored and white bars represent the mobility parallel and perpendicular to shearing, respectively. (c) Mobility anisotropy based on mobility values reported in (b).

3. CONCLUSION

In this work the ability of a micropillar blade capable of producing an otherwise non-present extensional flow field to align polymer chains during the deposition of a neat DPP-based polymer was evaluated. It was shown that an adequately large extensional flow field is successful in increasing polymer chain alignment and subsequently, thin film crystallinity. From electrical measurements of a 17 kDa molecular weight DPP-TT polymer it appears that polymer chain alignment can induce a faster charge transport in solution sheared films, but there is a competition between drying dynamics during shearing and polymer chain alignment, which results in a reduction in charge transport mobility and mobility anisotropy for films deposited in the LL regime. These findings were extended to polymers of varying chain length, where it was observed that the ability of an extensional flow field to align polymer chains is dependent on polymer chain length. In particular, polymers of sufficiently high molecular weight may be resistant to chain alignment and extension by extensional flow due to their properties in the solution state (e.g. on chain entanglements and aggregation state). Finally, it was shown that the effect of alignment on charge transport anisotropy increases with increasing chain length, likely due to the importance of "tie molecules" that bridge crystallites and allow for percolation down the polymer backbone in creating a fast charge transport in PSCs.

4. EXPERIMENTAL METHODS

4.1 Materials preparation

DPP-TT polymers were synthesized following previously reported methods by Stille coupling polymerization of 3,6-bis-(5-bromo-thiophene-2-yl)-N,N-bis(2-octyl-1-dodecyl)-1,4-dioxo-pyrrolo[3,4-c]pyrrole and 2,5-bis(trimethylstannyl)-thieno[3,2-b]thiophene.[52]

4.2 Blade Fabrication

Pillar structures were patterned using photoresists and a Cr mask layer was applied. Features were etched using dry ion etching (PlasmaTherm-DSE) to ~20 μm. Photoresist was washed away with acetone. The patterend silicon was treated with oxygen plasma for 1 minute at 150W and spincoated with 0.1 vol.% OTS/trichloroethylene solution and left overnight in an ammonia purged atmosphere. Patterned wafers were sonicated in toluene for 15 min and dried with nitrogen.

4.3 Solution Shearing Deposition

DPP-TT in chlorobenzene solution was prepared at 25, 10, and 5 mg/mL for Mn 10 kDa, 17 kDa, and 32 kDa DPP-TT, respectively, and were capped and pre-heated overnight at ~ 90 °C. Films were deposited onto 1.5x2 cm OTS-modified Si/SiO_2 substrates. The OTS monolayer was etched from the edge using a 1x1.5 cm PDMS stamp and oxygen plasma at 150 W for 5 seconds. During blade coating substrates were maintained at ~65 °C. 10 μL of solution was deposited per film of an area of 3 cm^2. The silicon reference blade was positioned 15 μm from the surface. All micropillar blades were placed to allow for 15 μm between the substrate and the largest blade feature. A front facing camera was used to ensure that the gap distance was constant between samples and that the gap did not vary in size across the width of the substrate. All blades used were placed at a 10° angle to the substrate. All films were annealed at 150 °C for 1 h.

4.4 Material Characterizations

Film thickness was measured by profilometer (Bruker Dektak 150). AFM measurements were performed in tapping-mode (Nanoscope III Digittal Instruments/Veeco Metrology Group). Polarized UV-Visible absorption spectra were measured using Agilent Cary 6000i UV/vis/NIR spectroscope with polarizer crystal. A sample area approximately 5x5 mm was measured. X-ray diffraction patterns were collected at beamline 11-3 and 7-2 at the Stanford Synchrotron Radiation Light Source (SSRL) with a beam energy of 12.7 and 14 keV, respectively. An incident angle of 0.12° was set. All x-ray samples were taken in Helium purged environments and cut to be roughly 1x1 cm in size. Intensity at each rotation angle was normalized according to previously reported methods.[16]

4.5 Device Fabrication/Testing

Bottom gate/top contact devices were fabricated by evaporating 40 nm Au contacts on PSC layer. The channel length and width are 50 and 1000 μm, respectively. All measurements were carried out in ambient conditions using a Keithley 4200-SCS. Reliability factors were calculated using previously reported methods.[47]

Supporting Information.

UV-Vis absorption spectra (**Figure S1 and S6b**); 2D GIWAXS patterns (**Figures S3 and S7**); AFM phase measurements (**Figures S4 and S8**); viscosity measurements (**Figure S6a**) ; additional transfer and output curves (**Figures S5 and S9**)

AUTHOR INFORMATION

Corresponding Author

*Email: zbao@stanford.edu

Author Contributions

The manuscript was written through contributions of all authors. All authors have given approval to the final version of the manuscript.

Notes

The authors declare no competing financial interest

ACKNOWLEDGMENT

Part of this work was performed at the Stanford Nano Shared Facilities (SNSF), supported by the National Science Foundation under award ECCS-1542152. GIXD measurements were carried out at the Stanford Synchrotron Radiation Laboratory (SSRL), a national user facility operated by Stanford University on behalf of the U.S. Department of Energy, Office of Basic Energy Sciences.

REFERENCES

(1) Tsao, H. N.; Cho, D.; Andreasen, J. W.; Rouhanipour, A.; Breiby, D. W.; Pisula, W.; Müllen, K. The Influence of Morphology on High-Performance Polymer Field-Effect Transistors. *Adv. Mater*. **2009**, *21* (2), 209–212.

(2) Yuan, Y.; Giri, G.; Ayzner, A. L.; Zoombelt, A. P.; Mannsfeld, S. C. B.; Chen, J.; Nordlund, D.; Toney, M. F.; Huang, J.; Bao, Z. Ultra-High Mobility Transparent Organic Thin Film Transistors Grown by an off-Centre Spin-Coating Method. *Nat. Commun*. **2014**, *5*, 1–9.

(3) Ro, H. W.; Downing, J. M.; Engmann, S.; Herzing, A. A.; Delongchamp, D. M.; Richter, L. J.; Mukherjee, S.; Ade, H.; Abdelsamie, M.; Jagadamma, L. K.; Amassian, A.. Morphology Changes upon Scaling a High-Efficiency, Solution-Processed Solar Cell. *Energy Environ. Sci.* **2016**, *9* (9), 2835–2846.

(4) Giri, G.; Delongchamp, D. M.; Reinspach, J.; Fischer, D. A.; Richter, L. J.; Xu, J.; Benight, S.; Ayzner, A.; He, M.; Fang, L.; Gi, X.; Toney, M.F.; Bao, Z. Effect of Solution Shearing Method on Packing and Disorder of Organic Semiconductor Polymers. *Chem. Mater.* **2015**, *27* (7), 2350–2359.

(5) Pierre, A.; Sadeghi, M.; Payne, M. M.; Facchetti, A.; Anthony, J. E.; Arias, A. C. All-Printed Flexible Organic Transistors Enabled by Surface Tension-Guided Blade Coating. *Adv. Mater.* **2014**, *26* (32), 5722–5727.

(6) Niazi, M. R.; Li, R.; Qiang Li, E.; Kirmani, A. R.; Abdelsamie, M.; Wang, Q.; Pan, W.; Payne, M. M.; Anthony, J. E.; Smilgies, D. M.; Sigurdur, T.T.; Giannelis, E.P.; Amassian, A.

Solution-Printed Organic Semiconductor Blends Exhibiting Transport Properties on Par with Single Crystals. *Nat. Commun*. **2015**, *6*, 1–10.

(7) Chu, P. H.; Kleinhenz, N.; Persson, N.; McBride, M.; Hernandez, J. L.; Fu, B.; Zhang, G.; Reichmanis, E. Toward Precision Control of Nanofiber Orientation in Conjugated Polymer Thin Films: Impact on Charge Transport. *Chem. Mater*. **2016**, *28* (24), 9099–9109.

(8) Wu, D.; Kaplan, M.; Ro, H. W.; Engmann, S.; Fischer, D. A.; DeLongchamp, D. M.; Richter, L. J.; Gann, E.; Thomsen, L.; McNeill, C. R.; Zhang, X. Blade Coating Aligned, High-Performance, Semiconducting-Polymer Transistors. *Chem. Mater*. **2018**, *30* (6), 1924-1936.

(9) Patel, S. N.; Su, G. M.; Luo, C.; Wang, M.; Perez, L. A.; Fischer, D. A.; Prendergast, D.; Bazan, G. C.; Heeger, A. J.; Chabinyc, M. L.; Kramer, E.J. NEXAFS Spectroscopy Reveals the Molecular Orientation in Blade-Coated Pyridal[2,1,3]thiadiazole-Containing Conjugated Polymer Thin Films. *Macromolecules* **2015**, *48* (18), 6606–6616.

(10) Molina-Lopez, F.; Wu, H.; Wang, G. N.; Yan, H.; Shaw, L.; Xu, J.; Toney, M. F.; Bao, Z. Enhancing Molecular Alignment and Charge Transport of Solution-Sheared Semiconducting Polymer Films by the Electrical-Blade Effect. *Adv. Electron. Mater.* **2018**, 1800110, 1–12.

(11) Diao, Y.; Tee, B. C. K.; Giri, G.; Xu, J.; Kim, D. H.; Becerril, H. A.; Stoltenberg, R. M.; Lee, T. H.; Xue, G.; Mannsfeld, S. C. B.; Bao, Z. Solution Coating of Large-Area Organic Semiconductor Thin Films with Aligned Single-Crystalline Domains. *Nat. Mater*. **2013**, *12* (7), 665–671.

(12) Diao, Y.; Lenn, K. M.; Lee, W. Y.; Blood-Forsythe, M. A.; Xu, J.; Mao, Y.; Kim, Y.; Reinspach, J. A.; Park, S.; Aspuru-Guzik, A.; Xue, G.; Clancey, P.; Bao, Z., Mannsfeld, S.C.B.

Understanding Polymorphism in Organic Semiconductor Thin Films through Nanoconfinement. *J. Am. Chem. Soc*. **2014**, *136* (49), 17046–17057.

(13) Xiao, C.; Kan, X.; Liu, C.; Jiang, W.; Zhao, G.; Zhao, Q.; Zhang, L.; Hu, W.; Wang, Z.; Jiang, L. Controlled Formation of Large-Area Single-Crystalline TIPS-Pentacene Arrays through Superhydrophobic Micropillar Flow-Coating. *J. Mater. Chem. C* **2017**, *5* (10), 2702–2707.

(14) Kim, J. O.; Lee, J. C.; Kim, M. J.; Noh, H.; Yeom, H. I.; Ko, J. B.; Lee, T. H.; Ko Park, S. H.; Kim, D. P.; Park, S. Inorganic Polymer Micropillar-Based Solution Shearing of Large-Area Organic Semiconductor Thin Films with Pillar-Size-Dependent Crystal Size. *Adv. Mater.* **2018**, *30* (29), 1–7.

(15) Wang, G.; Chu, P. H.; Fu, B.; He, Z.; Kleinhenz, N.; Yuan, Z.; Mao, Y.; Wang, H.; Reichmanis, E. Conjugated Polymer Alignment: Synergisms Derived from Microfluidic Shear Design and UV Irradiation. *ACS Appl. Mater. Interfaces* **2016**, *8* (37), 24761–24772.

(16) Diao, Y.; Zhou, Y.; Kurosawa, T.; Shaw, L.; Wang, C.; Park, S.; Guo, Y.; Reinspach, J. A.; Gu, K.; Gu, X.; Tee, B.C.K.; Pang, C.; Yan, H.; Zhao, D.; Toney, M.F.; Mannsfeld, S.C.B.; Bao, Z. Flow-Enhanced Solution Printing of All-Polymer Solar Cells. *Nat. Commun.* **2015**, *6*, 1–10.

(17) Venkateshvaran, D.; Nikolka, M.; Sadhanala, A.; Lemaur, V.; Zelazny, M.; Kepa, M.; Hurhangee, M.; Kronemeijer, A. J.; Pecunia, V.; Nasrallah, I.; Romanov, I.; Broch, K.; McCulloch, I.; Emin, D.; Olivier, Y.; Cornil, J.; Beljonne, D.; Sirringhaus, H. Approaching Disorder-Free Transport in High-Mobility Conjugated Polymers. *Nature* **2014**, *515* (7527), 384–388. https://doi.org/10.1038/nature13854.

(18) Gu, K.; Snyder, C. R.; Onorato, J.; Luscombe, C. K.; Bosse, A. W.; Loo, Y. L. Assessing the Huang-Brown Description of Tie Chains for Charge Transport in Conjugated Polymers. *ACS Macro Lett.* **2018**, *7* (11), 1333–1338.

(19) Noriega, R.; Rivnay, J.; Vandewal, K.; Koch, F. P. V; Stingelin, N.; Smith, P.; Toney, M. F.; Salleo, A. A General Relationship between Disorder, Aggregation and Charge Transport in Conjugated Polymers. *Nat. Mater*. **2013**, *12* (11), 1038–1044.

(20) Podzorov, V. Long and Winding Polymeric Roads. *Nat. Mater*. **2013**, *12* (11), 947–948.

(21) Mollinger, S. A.; Salleo, A.; Spakowitz, A. J. Anomalous Charge Transport in Conjugated Polymers Reveals Underlying Mechanisms of Trapping and Percolation. *ACS Cent. Sci.* **2016**, *2* (12), 910–915.

(22) Mollinger, S. A.; Krajina, B. A.; Noriega, R.; Salleo, A.; Spakowitz, A. J. Percolation, Tie-Molecules, and the Microstructural Determinants of Charge Transport in Semicrystalline Conjugated Polymers. *ACS Macro Lett*. **2015**, *4* (7), 708–712.

(23) Chew, A. R.; Ghosh, R.; Pakhnyuk, V.; Onorato, J.; Davidson, E. C.; Segalman, R. A.; Luscombe, C. K.; Spano, F. C.; Salleo, A. Unraveling the Effect of Conformational and Electronic Disorder in the Charge Transport Processes of Semiconducting Polymers. *Adv. Funct. Mater.* **2018**, *28*, 1804142, 1–9.

(24) Xu, J.; Wu, H.; Zhu, C.; Ehrlich, A.; Shaw, L.; Nikolka, M.; Wang, S.; Molina-lopez, F.; Gu, X.; Luo, S.; Zhou, D.; Kim, Y.H.; Wang, G.J.N.; Gu, K.; Feig, V.R.; Chen, S.; Kim, Y.; Katsumata, T.; Zhen, Y.Q.; Yan, H.; Chung, J.W.; Lopez, J.; Murmann, ,B.; Bao, Z. Multi-Scale

Ordering in Highly Stretchable Polymer Semiconducting Films. *Nat. Mater*. **2019,** *18* (6), 594-601.

(25) Larson, R. G. Flow-Induced Mixing, Demixing, and Phase Transitions in Polymeric Fluids. *Rheol. Acta* **1992**, *31* (6), 497–520.

(26) Laufer, Z.; Jalink, H. L.; Staverman, A. J. Time Dependence of Shear and Normal Stresses of Polystyrene and Poly(Ethylene Oxide) Solutions. *J Polym Sci Part A-1 Polym Chem* **1973**, *11* (11), 3005–3015.

(27) Pennings, A. J.; van der Mark, J. M. A. A.; Kiel, A. M. Correction of the Paper Hydrodynamically Induced Crystallization of Polymers from Solution. *Kolloid-Zeitschrift Zeitschrift für Polym*. **1970**, *238* (1–2), 544.

(28) Lamberti, G. Flow Induced Crystallization of Polymers. *Chem. Soc. Rev*. **2014**, *43* (7), 2240–2252. https://doi.org/10.1039/C3CS60308C.

(29) Wie, J. J.; Nguyen, N. A.; Cwalina, C. D.; Liu, J.; Martin, D. C.; Mackay, M. E. Shear-Induced Solution Crystallization of poly(3-Hexylthiophene) (P3HT). *Macromolecules* **2014**, *47* (10), 3343–3349.

(30) Wang, G.; Persson, N.; Chu, P. H.; Kleinhenz, N.; Fu, B.; Chang, M.; Deb, N.; Mao, Y.; Wang, H.; Grover, M. A.; Reichmanis, E. Microfluidic Crystal Engineering of π-Conjugated Polymers. *ACS Nano* **2015**, *9* (8), 8220–8230.

(31) Shaw, L.; Hayoz, P.; Diao, Y.; Reinspach, J. A.; To, J. W. F.; Toney, M. F.; Weitz, R. T.; Bao, Z. Direct Uniaxial Alignment of a Donor-Acceptor Semiconducting Polymer Using Single-Step Solution Shearing. *ACS Appl. Mater. Interfaces* **2016**, *8* (14), 9285–9296.

(32) Mcbride, M.; Persson, N. E.; Keane, D.; Bacardi, E.; Reichmanis, E.; Grover, M. A. A Polymer Blend Approach for Creation of Effective Conjugated Polymer Charge Transport Pathways. *ACS Appl. Mater. Intefaces* **2018,** *10* (42), 36464-36474.

(33) Trefz, D.; Gross, Y. M.; Dingler, C.; Tkachov, R.; Hamidi-sakr, A.; Kiriy, A.; Mcneill, C. R.; Brinkmann, M.; Ludwigs, S. Tuning Orientational Order of Highly Aggregating P(NDI2OD-T2) by Solvent Vapor Annealing and Blade Coating. *Macromolecules* **2018**, *52*, 43–54.

(34) Le Berre, M.; Chen, Y.; Baigl, D. From Convective Assembly to Landau - Levich Deposition of Multilayered Phospholipid Films of Controlled Thickness. *Langmuir* **2009**, *25* (5), 2554–2557.

(35) Gather, M. C.; Bradley, D. D. C. An Improved Optical Method for Determining the Order Parameter in Thin Oriented Molecular Films and Demonstration of a Highly Axial Dipole Moment for the Lowest Energy π-Π* Optical Transition in Poly(9,9- Dioctylfluorene-Co-Bithiophene). *Adv. Funct. Mater*. **2007**, *17* (3), 479–485.

(36) Köhler, A.; dos Santos, D. A.; Beljonne, D.; Shuai, J.-L.; Brédas, A. B.; Kraus, A.; Müllen, K.; Friend, R.H.; Charge Separation in Localized and Localized Electronic States in Polymeric Semiconductors. *Nature* **1998**, *392*, 903-906.

(37) Wang, W.; Guo, S.; Herzig, E. M.; Sarkar, K.; Schindler, M.; Magerl, D.; Philipp, M.; Perlich, J.; Muller-Büschbaum, P. Investigation of morphological degradation of P3HT:PCBM bulk heterojunction films exposed to long-term host solvent vapor. *J. Mater. Chem. A* **2016**, *4*, 3743-3753.

(38) Shaw, L.; Yan, H.; Gu, X.; Hayoz, P.; Weitz, R. T.; Kaelblein, D.; Toney, M. F.; Bao, Z. Microstructural Evolution of the Thin Films of a Donor-Acceptor Semiconducting Polymer Deposited by Meniscus-Guided Coating. *Macromolecules* **2018**, *51* (11), 4325–4340.

(39) Tsao, H. N.; Cho, D. M.; Park, I.; Hansen, M. R.; Mavrinskiy, A.; Yoon, D. Y.; Graf, R.; Pisula, W.; Spiess, H. W.; Müllen, K. Ultrahigh Mobility in Polymer Field-Effect Transistors by Design. *J. Am. Chem. Soc*. **2011**, *133* (8), 2605–2612.

(40) Ge, Q.; Newbloom, G. M.; Zhang, F.; Mohammadi, E.; Strzalka, J. W.; Pozzo, L. D.; Mei, J.; Diao, Y. Understanding Interfacial Alignment in Solution Coated Conjugated Polymer Thin Films. *ACS Appl. Mater. Interfaces* **2017**, *33* (9), 27863-27874

(41) Kline, R. J.; McGehee, M. D.; Kadnikova, E. N.; Liu, J.; Fréchet, J. M. J.; Toney, M. F. Dependence of Regioregular poly(3-Hexylthiophene) Film Morphology and Field-Effect Mobility on Molecular Weight. *Macromolecules* **2005**, *38* (8), 3312–3319.

(42) Kline, R. J.; McGehee, M. D.; Kadnikova, E. N.; Liu, J.; Fréchet, J. M. J. Controlling the Field-Effect Mobility of Regioregular Polythiophene by Changing the Molecular Weight. *Adv. Mater*. **2003**, *15* (18), 1519–1522.

(43) Niu, W.; Wu, H. C.; Matthews, J. R.; Tandia, A.; Li, Y.; Wallace, A. L.; Kim, J.; Wang, H.; Li, X.; Mehrotra, K.; Bao, Z.; He, M. Synthesis and Properties of Soluble Fused Thiophene Diketopyrrolopyrrole-Based Polymers with Tunable Molecular Weight. *Macromolecules* **2018**, *51* (23), 9422–9429.

(44) Noriega, R.; Salleo, A.; Spakowitz, A. J. Chain Conformations Dictate Multiscale Charge Transport Phenomena in Disordered Semiconducting Polymers. *Proc. Natl. Acad. Sci.* **2013**, *110* (41), 16315–16320.

(45) Grozema, F. C.; Siebbeles, L. D. A. Charge Mobilities in Conjugated Polymers Measured by Pulse Radiolysis Time-Resolved Microwave Conductivity: From Single Chains to Solids. J. *Phys. Chem. Lett.* **2011**, *2* (23), 2951–2958.

(46) Bartelt, J. A.; Douglas, J. D.; Mateker, W. R.; Labban, A. El; Tassone, C. J.; Toney, M. F.; Fréchet, J. M. J.; Beaujuge, P. M.; McGehee, M. D. Controlling Solution-Phase Polymer Aggregation with Molecular Weight and Solvent Additives to Optimize Polymer-Fullerene Bulk Heterojunction Solar Cells. *Adv. Energy Mater.* **2014**, *4* (9), 1–11.

(47) Scharsich, C.; Lohwasser, R. H.; Sommer, M.; Asawapirom, U.; Scherf, U.; Thelakkat, M.; Neher, D.; Köhler, A. Control of Aggregate Formation in poly(3-Hexylthiophene) by Solvent, Molecular Weight, and Synthetic Method. *J. Polym. Sci. Part B Polym. Phys*. **2012**, *50* (6), 442–453.

(48) Gu, X.; Shaw, L.; Gu, K.; Toney, M. F.; Bao, Z. The Meniscus-Guided Deposition of Semiconducting Polymers. *Nat. Commun*. **2018**, *9* (1), 534.

(49) Lee, W.Y.; Giri, G.; Diao, Y.; Tassone, C.J.; Matthew, J.R.; Sorensen, M.L.; Mannsfeld, S.C.B.; Chen, W.C.; Font, H.H.; Tok, J.B.H.; Toney, M.F.; He, M.; Bao, Z. Effect of Non-Chlorinated Mixed Solvents on Charge Transport and Morphology of Solution-Processed Polymer Field-Effect Transistors. *Adv. Funct. Mater.* **2014**, *24* (23), 3524-3534.

(50) Choi, H. H.; Cho, K.; Frisbie, C. D.; Sirringhaus, H.; Podzorov, V. Critical Assessment of Charge Mobility Extraction in FETs. *Nat. Mater.* **2017**, *17* (1), 2–7.

(51) Bucella, S. G.; Luzio, A.; Gann, E.; Thomsen, L.; McNeill, C. R.; Pace, G.; Perinot, A.; Chen, Z.; Facchetti, A.; Caironi, M. Macroscopic and high-throughput printing of aligned nanostructured polymer semiconductors for MHz large-area electronics. *Nat. Commun.* **2015**, *6*, 8394.

(52) Wang, G. N.; Shaw, L.; Xu, J.; Kurosawa, T.; Schroeder, B. C.; Oh, J. Y.; Benight, S. J.; Bao, Z. Inducing Elasticity through Oligo-Siloxane Crosslinks for Intrinsically Stretchable Semiconducting Polymers. *Adv. Funct. Mate*r. **2016**, *26,* 7254–7262.

TOC GRAPHIC

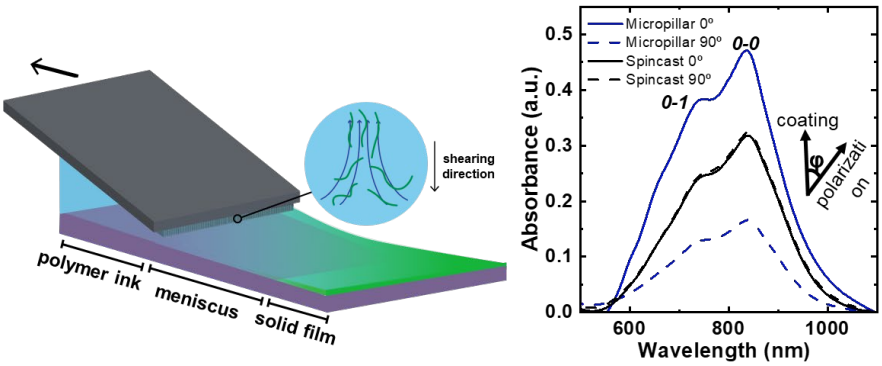
shearing direction
polymer ink
meniscus
solid film
Micropillar 0º
Micropillar 90º
Spincast 0º
Spincast 90º
0-0
0-1
coating
polarizati on
Absorbance (a.u.)
Wavelength (nm)
0.0
0.1
0.2
0.3
0.4
0.5
600
800
1000